Int. J. Heat Mass Transfer. Vol. 36, No. 11, pp. 2805–2813, 1993
Printed in Great Britain

0017-9310/93 $6.00 + 0.00

Freezing of aqueous sodium chloride solution saturated packed bed from a vertical wall of a rectangular cavity

J. CHOI and R. VISKANTA

Heat Transfer Laboratory, School of Mechanical Engineering, Purdue University, West Lafayette, IN 47907, U.S.A.

(*Received* 29 *June* 1992 *and in final form* 25 *November* 1992)

Abstract—Freezing of an aqueous sodium chloride (H_2O–NaCl) solution saturating a packed bed of glass spheres is investigated experimentally. Experiments are conducted on the hypoeutectic side, and the cold wall temperature is lower than the eutectic point. Spherical soda-lime glass beads 2.85 mm and 6 mm in average diameter constituted the packed bed. The effects of initial salt concentration, superheat and bead diameter are investigated. Three distinct regions came into existence during the freezing process. Supercooling was observed only at early times of the freezing process for an experiment with 5% initial salt concentration. However, small supercooling was observed throughout the freezing process for the 15% initial salt concentration experiment. Reheating of the mixture was intensified with an increase in the bead diameter, initial salt concentration, and near the vertical hot wall. At the end of the freezing process, remelting was observed only at the mush–liquid interface for the 10–15% initial salt concentration experiments. Flow visualization experiment and mush–liquid interface observations revealed natural convection in the upper part of the liquid region. An enriched and stratified fluid layer existed in the bottom of the liquid region. The intensity of natural convection was affected by both the Darcy and modified Rayleigh numbers.

INTRODUCTION

FREEZING of multicomponent systems saturating a solid permeable matrix is of considerable geophysical and technological interest. Examples of such processes include seasonal freezing of soil which occurs beneath roads, airstrips, buried utility lines and seasonal ice surfaces in cold climates. Long term freezing can occur beneath chilled pipelines, cryogenic storage tanks and year-round surfaces. In addition, artificial freezing of ground as a construction technique for poor soils has been used in practice for some time. Phenomena occurring during the freezing of aqueous binary solution are similar to those found in the solidification of metal alloys. Metallurgical applications include solidification of ingots, castings, and purification of materials. Other technological applications include freezing of mixtures and alloys saturating permeable matrix, manufacture of composite materials, production and preservation of foods, preservation of biological materials, etc. Reference is made to a recent review [1] for applications, and an extensive literature source on problems of phase change heat transfer in porous media.

The complexity of heat and mass transfer during freezing of a mixture saturating a porous matrix is mainly due to the conditions prevailing at the moving interface and the rejection of species. Three distinct regions exist in a system undergoing solidification. The process is further complicated by the structure (dendritic, columnar, etc.) of the frozen solid in the mushy region.

There is clearly fluid motion in the mushy region. The salt redistribution process occurring in the freezing of an NaCl solution was examined using microconductance probes fixed at stationary points in the test cell, and the factors responsible for controlling salt rejection were analyzed by Terwilliger and Dizio [2]. They found that two parameters control the redistribution process; one was the liquid phase interface concentration, which is determined by constitutional supercooling, and the other was the thermal driving force imposed on the system to initiate and maintain freezing. Phenomena of salt rejection during the freezing of a saline solution included in cells were investigated analytically and experimentally as a problem of heat and mass transfer with phase change [3]. It was found that solute rejection leads to depression of the freezing point in the liquid region of the cell and instabilities at the solid–liquid interface due to the constitutional supercooling. The instabilities at the interface give rise to the formation of a rough surface and occurrence of solute trapping on it. The growth of a solid–liquid two-phase region during selective freezing of a dilute, eutectic-forming, salt solution over a subcooled ice was investigated experimentally and theoretically [4]. The morphology of the two-phase region was photographed, and the kinetics of the solid–liquid interface was described. During the freezing of aqueous saline solution on a vertical wall of the rectangular cavity, the heavy solute-rich solution settled at the bottom of the test cell and formed a solutally stratified stable layer [5–8]. A liquid phase concentration layer developed ahead of the advancing

NOMENCLATURE

C	concentration of solute [wt%]
c_p	specific heat [J kg^{-1} K^{-1}]
Da	Darcy number, K/H^2
d	mean bead diameter [mm]
K	permeability [m^2]
k	thermal conductivity [W m^{-1} K^{-1}]
H	height of cavity [mm]
L	width of test cell [mm]
Ra^*	modified Rayleigh number, $g\beta(T_h - T_{eq})KH/\nu\alpha$
T	temperature [°C]
t	time [s]
x	horizontal coordinate [mm] (see Fig. 1)
z	vertical space coordinate measured from the bottom [mm].

Greek symbols

η	dimensionless distance, z/H
ξ	dimensionless distance, x/L
ϕ	porosity.

Subscripts

c	cold surface
eq	equilibrium corresponding to the initial salt concentration
h	hot surface
i	initial
l	liquid
s	solid.

solid–liquid interface was monitored using a Mach–Zehnder interferometer [9]. Natural convection fluid motion in the *n*-heptane was observed photographically using a Mach–Zehnder interferometer and a 10 mW He–Ne laser beam [10]. Recently, the effects of orientation and temperature of a cold surface during the freezing of pure water and ammonium chloride solution from below was studied experimentally [11, 12]. The temperature distributions, concentration variation in the liquid region, and the evolution of the liquidus positions during the freezing of aqueous saline solution saturated in a rectangular cell packed with spherical particles were studied by Okada and his co-workers [13, 14]. They found that the thermophysical properties did not affect significantly the permeability and phase change in the mushy region.

The present paper reports on an experimental investigation concerned with freezing of a packed bed of glass spheres saturated by a sodium chloride solution and cooled from a vertical side wall. The temperature and the mush/liquid interface position variations with time during the freezing process are also examined using a Stefan–Neumann type analysis in which natural convection is neglected. The paper reports on the effects of initial liquid concentration, superheat and bead diameter on temperature and concentration distributions and documents the fluid motion and the remelting phenomena of the mush–liquid interface. The main objective of the work is to obtain fundamental understanding of the heat and mass transfer processes during freezing and experimental data which could later be used to validate theoretical solidification models.

EXPERIMENTAL APPARATUS AND PROCEDURE

Freezing experiments were performed in a square cross-section test cell with inner dimensions of 149.2 mm in height and width and 73 mm in depth. Figure 1 shows schematically the experimental apparatus. The front, back, bottom and top surface of the test cell were made of acrylic plate. The vertical side surfaces were multi-pass heat exchangers made from copper plates and served as hot and cold walls. All acrylic walls were insulated with 50 mm thick Styrofoam, and two access windows were provided in the front and back of the insulation to allow for visual observation and photographing. Fifteen holes at equal intervals between $\xi = 0.07$ and $\eta = 0.93$ were drilled for the insertion of thermocouples, electrodes or hypodermic needles along the center line of both bottom and top walls of the test cell.

Ethyl-alcohol (100%) was circulated through the heat exchangers from two constant temperature baths. The entire test cell was placed on the aluminum plate with leveling screws to eliminate the effect of inclination of the test cell on the convection currents. Spherical soda-lime glass beads having average diameters of 2.85 mm and 6.0 mm constituted the porous medium. Experiments were performed with H_2O–NaCl solutions of different initial concentrations. Distilled and deionized water was mixed with requisite amount of research grade NaCl to obtain the desired salt concentrations. The solution was heated up to 80°C in order to degas the water. The degasified aqueous NaCl solution was carefully siphoned into the test cell without introducing any air bubbles into the system. Heat exchangers were connected through a valve system to two temperature baths (NESLAB ULT-80DD and HAAKE A 82). Through appropriate valve settings, the cold and hot walls could be maintained at the same temperature or different temperature. In the present experiments, it was impossible to achieve the steady-state by only maintaining the hot and cold walls at a same temperature before starting the experiments. This was because the fluid motion in the porous medium was very weak.

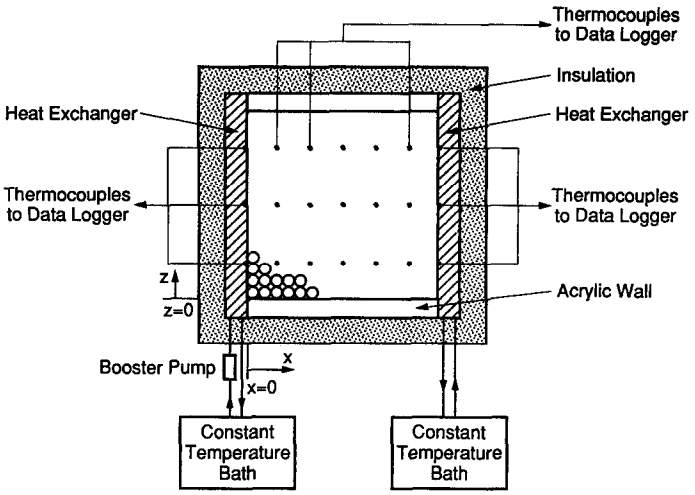

FIG. 1. Schematic diagram of the test cell.

To achieve the thermal equilibrium in the cavity, the solution was circulated using a very small capacity pump (1.5 m head). Equilibrium (uniform temperature and quiescent conditions) were reached in a short period of time (1–2 min) after the pump circulating the solution was shut off. The temperature of the hot vertical wall was maintained throughout the experiment at the same value as the initial liquid temperature.

An experiment was commenced by opening a valve to allow the preconditioned coolant to pass through the heat exchanger in the vertical cold wall. Thereafter, by adjusting the temperature of the constant temperature bath and the valves fitted to the discharge side of the heat exchanger, the cooled surface reached the desired temperature within 8 min from the initial liquid temperature. It took longer to reach the predetermined cold wall temperature than the experiments for freezing from above [15]. A booster pump was installed to increase the coolant flow rate through the cold wall on the discharge side of the constant temperature bath. Six thermocouples were placed along the surface of both heat exchangers to achieve the uniformity of the temperature along their faces, and 15 thermocouples were placed at the same position $\xi = 0.07, 0.26, 0.44, 0.62$, and 0.81 and $\eta = 0.11$, 0.5, and 0.89 on the center line of the test cell. All copper–constantan thermocouples (type-T) were calibrated with an accuracy of $\pm 0.1°C$. The wall temperatures of the heat exchangers and the temperature distribution in the test cell were recorded by an HP 3497 data acquisition system at predetermined time intervals (150 s).

During the freezing process one or two drops of solution were extracted by hypodermic needles to measure the concentration in the liquid and the mushy regions using the Kerno hand refractometer. Photographs for flow visualization and observation of the solid–mush interface were taken using a Nikon FE3 35 mm camera with a Nikon 55 mm Macrolens and Kodak 400 ASA Tmax film. Experiments for temperature measurement, flow visualization and concentration measurement were conducted separately to avoid heat gains or losses from the ambient and disturbance of the flow and temperature fields.

RESULTS AND DISCUSSION

Experimental conditions and flow visualization

Nine experiments were conducted with salt concentrations of 5, 10 and 15% by weight and different cold and hot wall temperatures and are listed in Table 1. Experiments 1–5 were conducted to measure temperature distributions. Experiments 6–8 were performed to measure the concentration variation, and experiment 9 was conducted to visualize the flow structure. The aqueous sodium chloride solution is a binary system with an eutectic point at $-21.12°C$ and eutectic composition of 23.31% by weight salt. All experiments were on the hypoeutectic composition side, and the cold wall temperature was lower than the eutectic point, and the hot wall temperature was higher than the liquidus temperature. Under these experimental conditions, three distinct regions come into existence as shown in Fig. 2. In the solid region adjacent to the vertical cold wall, the pores of the matrix are occupied by the frozen solid and appear white and are easily distinguishable from the mushy region. During freezing in the mushy region, which appeared grey, solid and liquid can coexist at various temperatures depending on the concentration of the binary alloy system. The liquid region adjacent to the hot wall is simply a part of the porous medium saturated with the saline solution that has not yet been solidified and appears colorless and transparent.

The flow visualization technique was based on the pH variation due to the electrolysis and consequent coloration of phenolphthalein in the aqueous solution

Table 1. Summary of experimental conditions

Exp.	C_i (%)	T_{eq} (°C)	d (mm)	T_c (°C)	$T_h = T_i$ (°C)	$T_i - T_{eq}$ (°C)	$T_{eq} - T_c$ (°C)	ϕ	$K \times 10^{-9}$ (m^2)	Ra^*
1	5	−3.0	2.85	−39.3	13.7	16.7	36.3	0.377	6.41	205.8
2	5	−3.0	6.0	−39.3	14.0	17.0	36.3	0.396	35.02	1163.0
3	5	−3.0	6.0	−39.2	22.5	25.5	36.2	0.396	35.02	1744.5
4	10	−6.5	6.0	−39.3	13.9	20.4	32.8	0.396	35.02	1641.3
5	15	−10.7	6.0	−39.3	13.8	24.5	28.6	0.396	35.02	1693.9
6	5	−3.0	6.0	−39.3	13.4	16.4	36.3	0.396	35.02	1121.9
7	10	−6.5	6.0	−39.3	13.8	20.3	32.8	0.396	35.02	1633.3
8	15	−10.7	6.0	−39.3	14.0	24.7	28.6	0.396	35.02	1707.7
9	5	−3.0	6.0	−39.3	13.9	16.9	39.3	0.396	35.02	1121.9

Experiments 1–5 were conducted to measure the temperature distributions.
Experiments 6–8 were performed to measure the concentration variation.
Experiment 9 was conducted for flow visualization.

around a cathode [16]. The simple electric circuit and amount of phenolphthalein solution recommended by Song and Viskanta [17] was utilized to generate a dye for flow visualization in the mushy and liquid regions. At each dye generating point, 0.9 mm O.D. stainless steel wire served as a cathode, and five electrodes were located at the positions of $\xi = 0.74$ and $\eta = 0.13, 0.31$, and 0.87, and $\xi = 0.87$ and $\eta = 0.13$ and 0.62. Figures 2(a) and (b) show the fluid motion for experiment 9 at $t = 6$ h and 6 h 30 min, respectively. They reveal the fact that an enriched stratified layer exists in the bottom of the liquid region. This finding is consistent with flow visualization results for freezing of aqueous salt solutions on a vertical cold wall [5–8]. With the progression of freezing, this layer increases in depth to form a stagnant region where there is no fluid motion. In this study, the layer diffused to the left and right rather than upwards and downwards. Counterclockwise currents were observed in the upper part of the liquid region, and the cells were affected by temperature and concentration gradients. The thermal and solutal convection currents were more intense at the hot wall than the mush–liquid interface. The intensity of natural convection circulation in the liquid region was influenced strongly by both the Darcy and modified Rayleigh numbers. The dye generated during the experiment was incorporated into the edge of the liquid region where the local solid fraction is vanishingly small. This finding indicates that the fluid penetrates the mushy region.

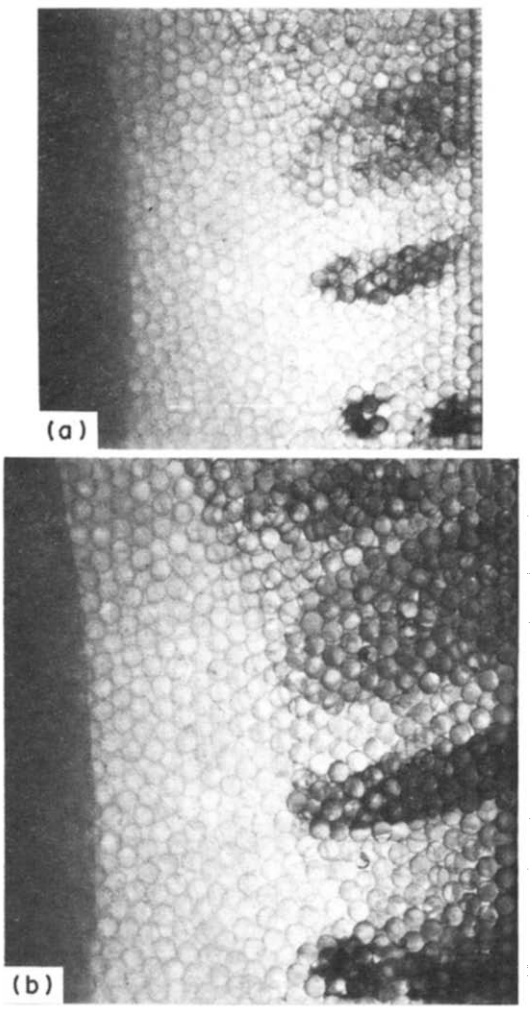

FIG. 2. Photographs showing the flow structure revealed by the pH flow visualization technique for experiment 9: (a) $t = 6$ h and (b) $t = 6.5$ h.

Comparison of heat conduction based model with experimental data

When an aqueous binary solution saturated with porous medium is frozen from a vertical cold wall in a rectangular cavity, the Stefan–Neumann type of analysis can be used to predict the temperature distributions in the cavity and the position of the mush–liquid interface. This type of theoretical analysis is well known in the literature [18–20]. For the sake of brevity, the governing equations and method of solution are not repeated here. In the analysis, the effect of the species diffusion on the freezing process is neglected, because the thermal diffusivity of the salt solutions is two orders of magnitude greater than the mass diffusivity. A one-dimensional conduction problem is considered with heat flow in the x-direction only. It is also assumed that local thermodynamic equilibrium exists. The average value of solid fraction in the mushy region, χ, used in the calculations is the

Table 2. Thermophysical properties used in the theoretical model

C_i (%)	5	10	15
k_s (W m^{-1} K^{-1})	2.285	2.285	2.285
k_l (W m^{-1} K^{-1})	0.5616	0.5564	0.5521
k_b (W m^{-1} K^{-1})	0.979	0.979	0.979
c_{ps} (J kg^{-1} K^{-1})	1953	1953	1953
c_{pl} (J kg^{-1} K^{-1})	3921	3720	3536
c_{pb} (J kg^{-1} K^{-1})	726.5	726.5	726.5
T_{eq} (°C)	−3.0	−6.5	−10.7
χ (—)	0.393	0.285	0.178
$\partial\chi/\partial T(1/K)$	−0.0433	−0.0388	−0.0354
ϕ (d = 6 mm)	0.396	0.396	0.396
ϕ (d = 2.85 mm)	0.377	0.377	0.377

arithmetic mean of the values at the solid–mushy and the mushy–liquid interface. The values of the properties used in the theoretical model are summarized in Table 2. The limitations of the model are well known (i.e. one-dimensional, neglect of thermal–solutal convection, etc.), but a comparison of model predictions with experimental data can be used to assess the relative importance of natural convection during the freezing process.

The effect of natural convection for 2.85 mm diameter beads ($\phi = 0.377$, $K = 6.41 \times 10^{-9}$ m^2) was comparatively smaller than for 6.0 mm ($\phi = 0.396$, $K = 35.02 \times 10^{-9}$ m^2) because of the lower permeability. For this reason, the data from experiment 1 are used to compare with the theoretical model, because the Stefan–Neumann type analysis neglects natural convection. Figure 3 shows the temperature distributions during freezing at positions $\eta = 0.11$, 0.5, and 0.89 and $\xi = 0.07$, 0.44, and 0.81 for experiment 1. In this figure, the dashed line represents the calculated temperature profiles using the Stefan–Neumann type analysis at the positions $\xi = 0.07, 0.44$, and 0.81, respectively. In the vicinity of the cold wall ($\xi = 0.07$), there is good agreement between the predicted and the measured temperatures and is uniformly good along the vertical cold wall. However, away from the cold wall (i.e. at $\xi = 0.44$ and 0.81) large discrepancies are evident between the predicted and measured temperatures in the liquid and mushy

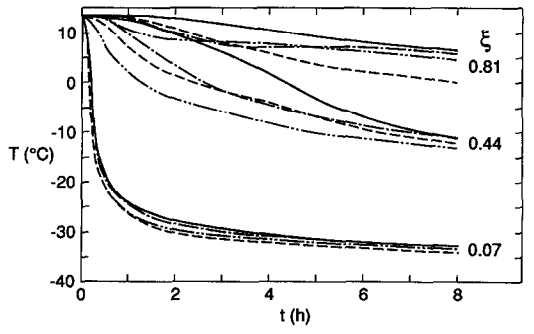

FIG. 3. Comparison of the predicted and measured temperatures for experiment 1 (——— $\eta = 0.89$; ——·—— $\eta = 0.5$; ——··—— $\eta = 0.11$; ——— theoretical model).

Table 3. Comparison of mushy–liquid interface positions for experiment 1 based on the theoretical model and experimental data measured at the positions of $\eta = 0$, 0.5, and 1.0

	Mush–liquid interface positions (mm)			
		Experimental		
Time (h)	Theoretical	$\eta = 0$	$\eta = 0.5$	$\eta = 1.0$
2	47	52	47	30
4	67	65	68	45
6	81	77	83	63
8	94	87	94	74

regions where the local solid reaction is relatively small. This is mainly the result of thermal and solutal convection. The temperatures at $\eta = 0.11$ were lower than those at $\eta = 0.89$ throughout the freezing process. These discrepancies suggest that the effect of natural convection was large in the upper part of the cavity and that there was a stagnant solutal layer in the lower part of the cavity (i.e. liquid region).

Table 3 shows a comparison of mush–liquid interface positions based on the theoretical model and experimental data measured at $\eta = 0$, 0.5, and 1.0 for experiment 1. At $\eta = 0.5$ the mush–liquid interface positions calculated theoretically agree well with the experimental data. At the bottom ($\eta = 0$) and top ($\eta = 1$) of the cavity, the measured mush–liquid interface positions are lower than predicted by the model. These differences are caused by the depression of the freezing temperature due to the stratified solutal layer and natural convection in the upper part of the cavity, respectively.

Results of parametric study

Figure 4 illustrates the effect of superheat on freezing of 6.0 mm diameter glass beads–aqueous system. During the freezing of a saline solution, the freezing point and superheat change continuously due to the rejection of solute from the liquidus into the melt. The superheat is the excess temperature of the binary alloy above its liquidus temperature and indicates the strength of thermally driven natural convection currents. In Fig. 4, the solid lines denote the data for experiment 2, and the dashed lines represent the data

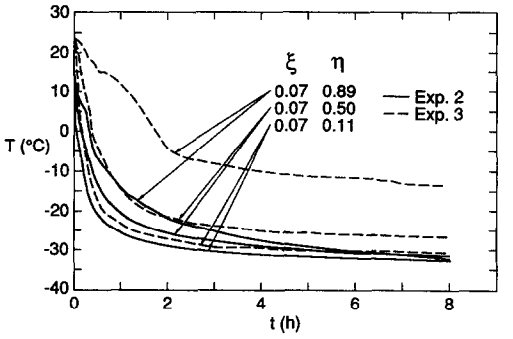

FIG. 4. Effect of liquid superheat for 6.0 mm diameter beads.

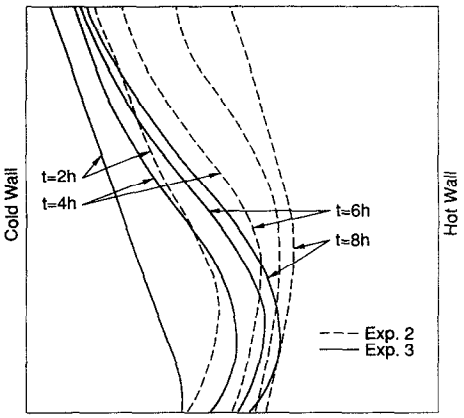

FIG. 5. Evolution of the mush–liquid interface for experiments 2 and 3.

for experiment 3 at the positions of $\xi = 0.07$ and $\eta = 0.11$, 0.5, and 0.89. The superheats for experiments 2 and 3 are 17.0°C and 25.5°C, respectively. The effect of the superheat is clearly discernible in the upper part of the cavity ($\eta = 0.89$) and decreases in the lower part of the cavity. At the upper part of the vertical cold and hot walls ($\xi = 0.07$, 0.81 and $\eta = 0.89$), the temperatures were strongly affected by vigorous natural convection flows.

Figure 5 compares the mush–liquid interface evolutions for experiments 2 and 3 at 2 h intervals during the freezing of a binary solution saturating a packed bed of spheres in the rectangular cavity. In this figure, the solid and dashed lines represent the mush–liquid interfaces (liquidus) for experiments 3 and 2, respectively. The local freezing rate of the upper part of the cavity was smaller than in the lower part as the superheat was increased. The shape of the mush–liquid interface showed that natural convection-driven currents dominated solidification as the superheat was increased and that a solutally stratified layer is created in the lower part of the liquid region, and the depth of this layer increases as freezing progresses. Thermally driven natural convection currents are stronger in the upper part of the cavity as the superheat is increased, and the depth of this layer increases with the freezing process. The thermally driven natural convection currents are stronger in the upper part of the cavity as the superheat is increased. As freezing continues, the stratified layer increases in depth, and the ridge where the local freezing rate is maximum moves progressively upwards. The shapes of the mush–liquid interface contours observed and their timewise evolutions are similar to those found during freezing of aqueous salt solutions on a vertical cold wall [5–8].

Figure 6 compares the temperature variations with time for $d = 2.85$ mm ($Da = 2.28 \times 10^{-7}$) and 6.0 mm ($Da = 15.7 \times 10^{-7}$) bead diameters at the five locations, $\eta = 0.5$ and $\xi = 0.07$, 0.26, 0.44, 0.62, and 0.81. In this figure, the dashed line represents the data for $d = 2.85$ mm (experiment 1) and solid lines are for

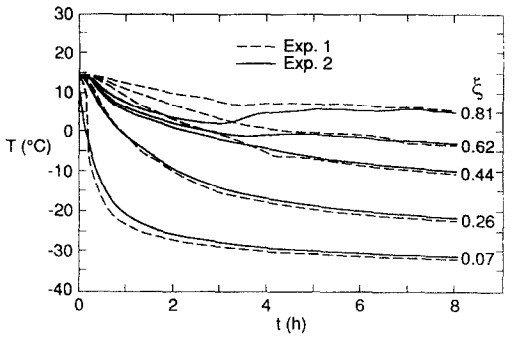

FIG. 6. Effect of bead diameter on the temperature vs time history for experiments 1 and 2.

$d = 6.0$ mm (experiment 2). In the upper part of the cavity ($\eta = 0.89$), the effect of bead diameter was clearly discernible, and temperature for $d = 2.85$ mm was lower than for $d = 6.0$ mm throughout the freezing process. Below the horizontal centerline of the cavity ($\eta = 0.11$ and 0.5), the temperatures for $d = 2.85$ mm were lower than for $d = 6.0$ mm near the cold wall. But, the temperatures in the vicinity of the hot wall were inverted, because of the low permeability. At the lower part of the cavity ($\eta = 0.11$), the effect of the bead diameter is very small compared to in the upper part.

Figure 7 compares the mush–liquid interface evolutions for experiment 1 ($d = 2.85$ mm) and experiment 2 ($d = 6.0$ mm) in 2 h intervals during the freezing process. In this figure, the solid line represents the mushy–liquid interface for $d = 6.0$ mm and the dashed line for $d = 2.85$ mm. Interface evolution for $d = 2.85$ mm beads shows that natural convection was very weak because of relatively low permeability. However, in the case of the porous medium formed by $d = 6.0$ mm beads, the local freezing rate of the lower part of the cavity was larger than in the upper part of the cavity. There was a solutally stratified layer in the lower part of the liquid region, and the thickness of the layer increased as the freezing progressed. Consequently, the ridges where the local freezing is maximum moved

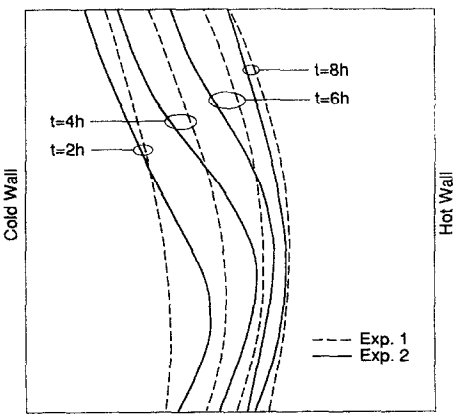

FIG. 7. Evolution of the mush–liquid interface for $d = 2.8$ mm (experiment 1) and $d = 6$ mm (experiment 2).

upwards from the bottom of the cavity. Note that at late times ($t = 8$ h) the mush–liquid interface positions for the two experiments are rather close and similar in shape to each other.

Figure 8 illustrates the effect of the initial salt concentration on the freezing rate by comparing the temperatures at selected locations for the $C_i = 5\%$ (experiment 2) and 10% (experiment 4). Experiments 2 and 4 are for the same bead diameter and cold and hot wall temperatures, but the initial salt concentrations are 5 and 10% by weight, respectively. Figure 8(a) reveals that there was little effect of the initial salt concentration at $\eta = 0.5$, but in the upper part of the cavity at $\eta = 0.89$ (Fig. 8(b)) the effect of the initial salt concentration was clearly discernible. The temperatures for $C_i = 5\%$ by weight are lower than those for $C_i = 10\%$ by weight. At the bottom of the cavity ($\eta = 0.11$), the temperature for $C_i = 10\%$ is lower than that for $C_i = 5\%$ during the early times of the freezing process. However, as the freezing progressed, there was little effect of the initial salt concentration on the temperatures. In the vicinity of the vertical cold wall ($\xi = 0.07$), temperatures for $C_i = 10\%$ are lower than those for $C_i = 5\%$ at the lower part of the cavity, but in the upper part of the cavity the temperatures became inverted because of vigorous natural convection.

Figure 9 shows the location of mush–liquid interface at $t = 2$ and 8 h after the freezing was initiated. In this figure the dashed line, dashed–dot line, and solid line represent the positions of the mush–liquid interface for $C_i = 5\%$ (experiment 2), 10% (experiment 4) and 15% (experiment 5) salt concentrations by weight, respectively. The global freezing rate (i.e. average frozen layer thickness) decreased, and the ridges moved downward with an increasing initial salt concentration. This is owing to the fact that natural convection was more vigorous, and the thickness of the solutally stratified layer decreased with a decrease in the initial salt concentration. The solutally stratified layer was thicker near the hot wall than at the mush–liquid interface as shown in Figs. 2(a) and (b). The solute rejected from the solid–liquid interface is transported through the mushy region to the liquidus by diffusion and natural convection and is redistributed in the unfrozen liquid region; therefore, the salt concentration in the liquid is increased from the initial value. A stratified, stagnant layer develops in the bottom part of the liquid region. This is owing to the fact that thermal and solutal convection was more vigorous, and the solutally stratified layer increased in depth with an increase in the initial salt concentration. The enriched solute may lead to constitutional supercooling in the melt.

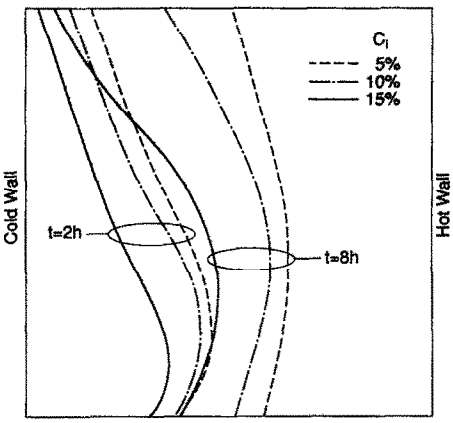

FIG. 9. Location of mush–liquid interface for $C_i = 5\%$ (experiment 2), 10% (experiment 4) and 15% (experiment 5) at $t = 2$ and 8 h.

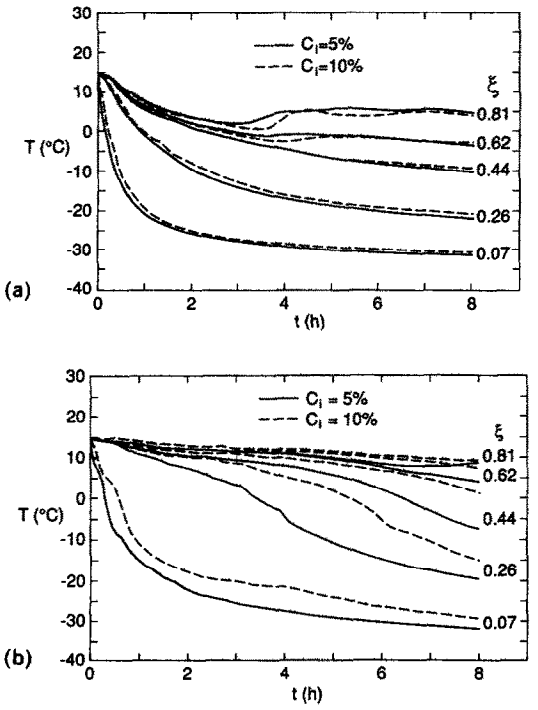

FIG. 8. Effect of initial salt concentration on the temperature vs time history for $C_i = 5\%$ (experiment 2) and 10% (experiment 4) at $\eta = 0.5$ (a) and at $\eta = 0.89$ (b).

In order to measure the concentration variation in the mushy and liquid regions, three experiments (experiments 6–8), with nearly the same cold and hot wall temperatures, and initial salt concentrations of 5, 10 and 15% by weight were performed. The porous medium was formed by 6.0 mm diameter glass beads. During the freezing process, one or two drops of solution were extracted by three hypodermic needles located at the positions of $\xi = 0.2$, 0.74 and $\eta = 0.13$ as well as $\xi = 0.74$ and $\eta = 0.87$ to measure the concentration variation in the liquid and mushy regions using a refractometer. As shown in Fig. 10, at position $\xi = 0.2$ and $\eta = 0.13$, the concentration in the mushy region increased rapidly at early times of the freezing process, but the rate of increase leveled off as the eutectic composition was approached. It took longer to reach the eutectic point from the initial salt concentration as the salt concentration was increased.

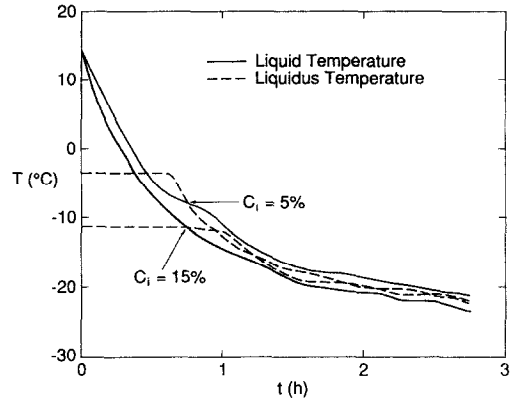

FIG. 10. Concentration variation with time in the mushy region at the position of $\xi = 0.20$ and $\eta = 0.13$.

This implies that the global freezing rate is increased with a decrease in the initial salt concentration. The same phenomenon was also observed in the study of freezing of aqueous sodium chloride solution saturated packed bed from above [15].

Figure 11 shows a comparison between the actual liquid and liquidus temperatures at the position of $\xi = 0.2$ and $\eta = 0.13$ during freezing of binary alloys with $C_i = 5$ and 15%. In these figures, the solid line represents the actual liquid temperature measured by a thermocouple, and the dashed line denotes the liquidus temperature corresponding to the measured concentration of saline solution during the freezing process. For $C_i = 5\%$ supercooling was observed at early times of the freezing process, but as the freezing continued the liquid temperature became higher than the liquidus temperature. For $C_i = 15\%$ by weight, the liquid temperature was lower than the liquidus temperature throughout the freezing process. An increase in the initial liquid concentration increased the rate of heat transfer because the thickness of the mushy region in the lower part of the cavity became smaller. The decreased rate of the mass diffusion was caused by the small difference in salt concentration between the solid–liquid interface and the liquid

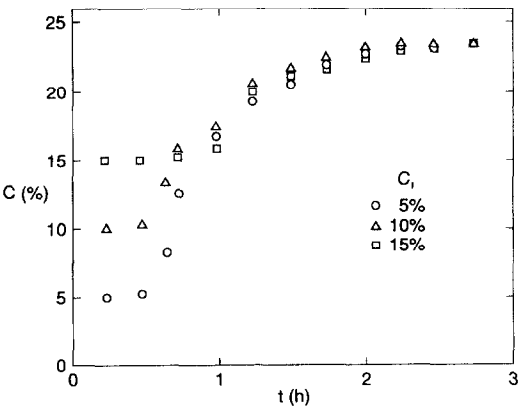

FIG. 11. Dependence of the liquid and liquidus temperatures on time.

region as freezing continued. Small supercooling was observed throughout the freezing process for $C_i = 15\%$. During the freezing with $C_i = 5$, 10 and 15% by weight, at the lower part of the liquid region ($\xi = 0.74$ and $\eta = 0.13$), the liquid concentration increased to 6.8, 12.8, and 18.9% by weight at 4 h after freezing was initiated. In the upper part of the liquid region ($\xi = 0.74$ and $\eta = 0.87$) the flow is driven by thermal convection, because concentration variations in the liquid are less than 0.2% by weight in salt. This means that a solutally stratified layer exists only in the bottom part of the liquid region. This layer is very stable and was not affected by natural convection flow. Due to its higher NaCl concentration, the liquidus temperature was depressed in the lower part of the cavity. Consequently, the local freezing rate adjacent to this solutally stratified layer was lower than in the middle part of the cavity. In the uncontaminated liquid region in the upper part of the cavity, there existed a counterclockwise natural convection flow cell caused by thermal buoyancy forces. The smaller thickness of the mushy zone near the top of the cavity is attributed to the thermal convection currents. Consequently, the local freezing rate is greatest at the bottom part of the vertical wall where the natural convection flow is weak, because the flow is downward along the mush liquid interface.

In experiment 1 reheating of the solution was not observed, except near the end of the freezing process at $\xi = 0.81$ and $\eta = 0.05$, because of relatively small permeability. The increase in temperature at the end of the process was very small (about 1°C). When the superheat was increased as in experiment 3, reheating of the solution was not observed throughout the freezing because of the strong natural convection currents. It was found that reheating of solution increased with an increase in the bead diameter, initial salt concentration near to the vertical hot wall. At the end of the freezing process, remelting was observed only at the mush–liquid interface for the experiments with $C_i = 10$ and 15% by weight salt but not for $C_i = 5\%$, and this occurred in the lower part of the ridge where the local freezing rate was maximum. It appears that this is caused by the reheating of the solution during the freezing process.

CONCLUDING REMARKS

A number of freezing experiments have been performed to investigate the effects of the liquid superheat, bead diameter and initial liquid concentration on the heat transfer and the interface positions during freezing from a vertical side wall of aqueous sodium chloride solutions saturating a porous medium. Flow visualization experiments have revealed the fact that a salt enriched stratified layer existed in the bottom part of the liquid region and that the natural convection currents were present in the upper part of the test cell. The intensity of the currents was strongly affected by the Darcy and the modified Rayleigh numbers.

Three distinct regions—solid, mushy and liquid—were observed near the cooled wall. The effect of superheat was clearly discernible and was affected by the vigorous natural convection flow at the upper part of the cavity and decreased near to the lower part of the cavity. With an increase in the superheat, the local freezing rate of the upper part of the cavity was smaller than the lower part and revealed a shape typical of solidification on a vertical wall which is influenced by natural convection currents. In the lower part of the test cell, the effect of the bead diameter was very small compared to the upper part, and the temperatures for 2.85 mm diameter beads were lower than those for the 6.0 mm beads only in the vicinity of the vertical cold wall.

The effect of initial salt concentration is clearly discernible in the upper part of the cavity, but there was little effect of the initial salt concentration, except at early times in the freezing process in the bottom part of the cavity. The average freezing rate decreased and the thickness of the solutally stratified layer increased as the initial salt concentration increased. For the experiment with $C_i = 5\%$, supercooling was observed only at early times of the freezing process, but for $C_i = 15\%$ supercooling was observed throughout the process. At the end of freezing, remelting was observed only at the lower part of the mush–liquid interface for experiments with $C_i = 10$ and 15%. This is attributed to the effect of reheating of the solution during the freezing.

Acknowledgements—The authors acknowledge the assistance of Mr M. Song in the performance of the experiments.

REFERENCES

1. R. Viskanta, Phase change heat transfer in porous media. In *Proceedings of the Third International Symposium on Cold Regions Heat Transfer* (Edited by J. P. Zarling), pp. 1–24. University of Alaska, Fairbanks, Alaska (1991).
2. P. Terwilliger and S. F. Dizio, Salt rejection phenomena in the freezing of saline solutions, *Chem. Engng Sci.* **25**, 1331–1349 (1970).
3. Y. Hayashi and T. Komori, Investigation of freezing of salt solutions in cells, *J. Heat Transfer* **101**, 459–464 (1979).
4. L. J. Fang, F. B. Cheung, J. H. Linehan and D. R. Pedersen, Selective freezing of a dilute salt solution on a cold ice surface, *J. Heat Transfer* **106**, 385–393 (1984).
5. S. Chellaiah and R. Viskanta, Freezing of salt solution on a vertical wall, *Exp. Heat Transfer* **1**, 181–195 (1988).
6. C. Beckermann and R. Viskanta, An experimental study of solidification of binary mixtures with double-diffusive convection in the liquid, *Exp. Thermal Fluid Sci.* **2**, 17–26 (1989).
7. S. Chellaiah, R. A. Water and M. A. Zampino, Solidification of an aqueous salt solution in the presence of thermosolutal convection. In *Proc. ASME/JSME Thermal Engineering Joint Conference* (Edited by J. R. Lloyd and Y. Kurosaki), Vol. 2, pp. 165–173. ASME, New York (1991).
8. M. A. Zampino, R. A. Waters and S. Chellaiah, An experimental study of freezing of binary solutions. In *ASME Proceedings of the National Heat Transfer Conference* (Edited by E. Hensel *et al.*), HTD-Vol. 159, pp. 37–45. ASME, New York (1991).
9. B. W. Grange, R. Viskanta and W. H. Stevenson, Diffusion of heat and solute during freezing of salt solutions, *Int. J. Heat Mass Transfer* **19**, 373–384 (1976).
10. P. D. Van Baren and R. Viskanta, Interferometric observation of natural convection during freezing from a vertical flat plate, *J. Heat Transfer* **102**, 375–378 (1980).
11. K. Sasaguchi and T. Matsufuji, Solid/liquid phase change heat transfer in porous media, *JSME Ser. B.* **57**, 1340–1346 (1991).
12. K. Sasaguchi, T. Noguchi and Y. Moriyama, An experimental study on solidification of a binary mixture. In *27th National Heat Transfer Symposium of Japan*, Vol. 1, pp. 253–255 (1990).
13. M. Okada and M. Murakami, Solidification of porous media saturated with aqueous solution in a rectangular cell. In *27th National Heat Transfer Symposium of Japan*, Vol. 1, pp. 241–243 (1990).
14. M. Okada, K. Matsutomo, M. Murakami and Y. Yabushita, Solidification of porous media saturated with aqueous solution in a rectangular cell. In *28th National Heat Transfer Symposium of Japan*, Vol. 1, pp. 304–306 (1991).
15. J. Choi and R. Viskanta, Freezing of aqueous sodium chloride solution saturated packed bed from above. In *Topics in National Heat Transfer—Vol. 2* (Edited by M. Toner, M. I. Flik and W. B. Webb *et al.*), HTD-Vol. 206-2, pp. 159–166. ASME, New York (1992).
16. M. Behnia and R. Viskanta, Natural convection flow visualization in irradiated water cooled by air flow over the surface. In *Natural Convection in Enclosures* (Edited by K. E. Torrance and I. Catton), pp. 17–26. ASME, New York (1980).
17. M. Song and R. Viskanta, Natural convection flow and heat transfer between a fluid layer and an isotropic porous layer within a rectangular enclosure. In *Heat Transfer in Enclosures* (Edited by R. W. Douglass and R. J. Dallman), HTD-Vol. 177, pp. 1–12. ASME, New York (1991).
18. M. N. Ozisik, *Heat Conduction*, pp. 410–412. Wiley, New York (1980).
19. S. L. Braga and R. Viskanta, Solidification of a binary solution on a cold isothermal surface, *Int. J. Heat Mass Transfer* **33**, 745–754 (1990).
20. W.-Z. Cao and D. Poulikakos, Freezing of a binary alloy saturating a packed bed of spheres, *J. Thermophys. Heat Transfer* **5**, 46–53 (1991).